Proceedings of the Korean Nuclear Society Autumn Meeting
Seoul, Korea, October 1998

CFD Application on IRWST Hydrodynamic Analysis during the Sparger Air Venting

Y. I. Kim, Y. D. Hwang, H. Y. Kim, Y. Y. Bae, J. K. Park
Korea Atomic Energy Research Institute

ABSTRACT

A numerical study was performed using preleased FLUENT V4.5 to investigate the applicability of the CFD model for IRWST hydrodynamic analysis during the sparger air venting. Transient calculations were performed with the compressible VOF model on the selected ABB-Atom Unit Cell Test data. This study was mainly focused on the simulation of the bubble formation process in the water pool and time varying pressure history during the air venting from the sparger. The simulated peak pressure was over-predicted in general, but the main frequency is in good agreement with the simulated data. It was shown that there was a strong dependence on the mass discharge rate of the air trapped in the vent line. The peak pressure acceptable for the conservative evaluation of the sparger performance was obtained by reducing the air discharge velocity. This indicates that the proper estimations of the air venting velocity consistent with the sparger design and operating conditions is essential for the application of FLUENT V4.5 to the sparger performance analysis of KNGR.

1. Introduction

In Korean Next Generation Reactor (KNGR), a sparger is introduced to increase the quenching efficiency of steam and to alleviate probable pressure surge induced by the sudden discharge of the high pressure steam from Reactor Coolant System (RCS) during the postulated accident. When the Safety Relief Valve (SRV) opens, the steam flow from RCS compresses the air trapped in the discharge line, and accordingly increases the line pressure. The increased air pressure forces the water into the In-containment Refueling Water Storage Tank (IRWST) first. Following the expulsion of water, the compressed air in the line is forced out through the sparger into the IRWST and the steam discharge is followed. The phenomena involved in this process include water jets, pressure oscillations of the air bubble and pressure fluctuations related to steam condensation. These disturbances, in turn, produce hydrodynamic loads both on the structures submerged in the IRWST and on the IRWST boundaries. The sparger should be designed to produce the loads as low as possible, and the structures in and of the IRWST should be designed according to those loads. It is therefore essential to develop the means to predict the hydrodynamic loads associated with discharge process.

As a first step to develop the Computational Fluid Dynamic (CFD) model for the analysis of hydrodynamics in IRWST for KNGR, a numerical study was performed on the selected ABB-Atom Unit Cell Test data. ABB-Atom had used these data to

develop the sparger for boiling water reactor (BWR), which minimizes the pressure amplitudes in the suppression pool during relief valve operation[1]. Since the hydrodynamic load produced by the oscillation of air bubble, formed by the discharged air into the water pool, is significantly higher than that produced by the water jet or steam condensation, this study is focused on the prediction of air bubble behavior and associated pressure oscillation by computational fluid dynamic code. The analysis includes the prediction of air bubble formation and shape change, pressure history and its peak pressure. For the analysis FLUENT V4.5 (pre-released), the commercially available computational fluid dynamics code, was used.

2. Description of ABB-Atom Unit Cell Test

ABB-Atom Unit Cell Test data were chosen as a benchmark data to investigate the applicability of the FLUENT V4.5 for the sparger performance analysis of KNGR.

ABB-Atom used the Unit Cell Test[1] to investigate the performance of the sparger used in ABB-Atom Boiling Water Reactor (BWR). The experimental program consisted of the 1) measurement of dynamic pressure loads in the blowdown pipe and condensation tank during the transient phase of discharge, 2) investigation of the influence on the back-suction of water into the blowdown pipe after closure of the safety valve, and 3) study of the influence of increased pool temperature on the magnitude of the pressure oscillation in the tank.

The test was performed using a pop action pilot operated safety valve through which steam was discharged into a condensation tank. The inner diameter of the connecting pipe is 159 mm. The condensation pool is comprised of a steel tank containing 42 m^3 of water at atmospheric pressure. The steam was supplied with the mass flow rates of 26 and 34 kg/sec at 70 bar. The schematic of the test facility of ABB-Atom Unit Cell Test is shown in Figure 1.

The pressure histories in the tank measured at the locations just below the sparger head and the mid point between Load Reduction Ring(LRR) and sparger head were selected for simulation. These are designated as PT8 and PT10 in Figure 1(b), respectively.

3. Method of Analysis

FLUENT code has two different models for two phase flow analysis: the Volume Of Fraction (VOF) model and the Eulerian model. The pressure boundary conditions and compressibility of primary phase are available in VOF model[2], but these options are not available in current Eulerian model. Therefore, the VOF model was selected to simulate the bubble behavior formed by the discharged air into the Unit Cell, even though Eulerian two phase model seems to be more realistic according to visualization of the two phase flow from the individual orifices in sparger head. With a VOF representation, two effective bubbles are formed: one is at the load reduction ring and the second is at the sparger head. The air bubble represents the cluster of small bubbles like a bubble cloud. In the application of the VOF approach, the kinetic energy of the air flow is assumed to be converted to work energy against the inertia of the water efficiently.

3.1 Model Generation

Unit Cell Test tank including the sparger pipe is modeled in two-dimensional

axisymmetric coordinate. The air/water interface in the pipe modeled to be exist in the geometry modeling, while the steam/air interface reaches the inlet boundary sometime after SRV opening. The video of the Unit Cell Test shows that the general shape of the ensemble of air bubbles is roughly spherical at the sparger head and skirt-shaped at the Load Reduction Ring (LRR). This observation suggests the application a two-dimensional axisymmetric model for representation of sparger dynamics. The resulting grid geometry is shown in Figure 1(c).

The LRR and the sparger head are modeled as porous media. This approach artificially reduce the flow velocity and thus enhance the convergence of the solution. An inertial resistance factor is assigned to the porous media to maintain the proper pressure drop and mass flow rate across the region. The flow resistance of the porous media was estimated based on the expansion area and the inertial resistance of flow as summarized in Table 1. When the discharge velocity exceeds the critical velocity of air, the velocity is fixed at the critical velocity of the porous cell by assuming choking condition. The critical velocities used in the calculations are summarized in Table 2.

3.2 Computational Procedure

The moving interface of the air-water is simulated by automatic tracking, but the steam-air interface is controlled manually as a boundary condition. Only the primary phase, air in this model, is allowed to be compressible in FLUENT modeling. The steam component is specified as the incompressible fluid. The density of the steam phase is approximated to have the similar value of the compressed air. When the air-steam interface reaches down to the LRR or holes of the sparger head, the LRR and holes are blocked due to the limitation of the FLUENT code for steam condensation.

During the air venting through the sparger, the air pressure within the pipe reaches high pressure enough for choked flow at the LRR and sparger head and creates the additional discontinuity of flow. In order to cope with the flow discontinuities, the inlet conditions for air discharge are controlled in a piecewise manner. The procedure consists of the following steps.

Step 1 : Pressure rise at the air-water interface starts injection of the water through the LRR and sparger head.

Step 2 : The steam-air interface is formed in the computation domain when the air trapped in the sparger pipe passes through the inlet boundary completely. At this time, the steam is allowed to enter the computation domain through pipe inlet.

Step 3 : When the pressure difference across LRR reaches the choking condition, the discharge velocity of air at LRR is fixed at critical velocity.

Step 4 : When the pressure difference reaches the choking condition across the holes at the sparger head, the discharge velocity of air at sparger head is fixed at critical velocity.

Step 5 : The steam/air interface is permitted to pass through LRR and the sparger head. After the complete discharge of the air, the LRR and sparger head is blocked to prevent the inflow of incompressible steam which produces the non-physical pressure disturbances.

Transient calculations were performed following the procedures delineated above in piecewise manner. The results are described in the following section in detail.

4. Analysis Results

Transient calculation was performed with the VOF model to simulate the pressure histories for the selected case of the Unit Cell Test. The time step size of 5.0×10^{-4} sec was used while the simple flow pattern was maintained in the flow field. When the complicated flow pattern are developed, either of the reduced time step size of 2.0×10^{-4} or 1.0×10^{-5} sec is used to improve the solution convergence.

The solutions at each time step are considered to be converged when the normalized residuals of all dependent variables are smaller than the convergence criterion, 1×10^{-3}. The pressure histories for the cell corresponding to the locations designated as PT8 and PT10 in Figure 1(b) were monitored during the calculation.

Three cases were calculated to investigate the influences of the air discharge rate on pressure transients by varying the air discharge velocity through the sparger. Case A used critical velocity of pure air, 330 m/sec, at both of LRR and sparger head[4]. Case B and C were performed with the reduced critical velocity by assuming the discharge of air-water mixture. Case B used critical velocity of 100 m/sec at both locations of the LRR and sparger head. Case C used critical velocity of 100 m/sec at the LRR and 50 m/sec at the sparger head. The effects of the steam discharging(steam condensing) were not included in these calculations by blocking the LRR and/or sparger head when the steam-air interface reaches the LRR and/or sparger head. The introduction of the steam assumed as incompressible gas phase into the computation domain produces the non-physical pressure spikes. The critical velocities of air and its equivalent velocities used in the calculation are summarized in Table 2.

The calculated pressure histories of Case A, B and C are shown in Figures 3, 4 and 5, respectively. The FLUENT calculation reproduced the some of the basic features, in general, of the Unit Cell Test data. The main frequency and wave form of the pressure history reproduced the simulated data with good agreement in all three cases. The maximum peak pressure was over-predicted the simulated Unit Cell Test and it shows a strong dependence on the air discharge rate. The peak pressures decreased significantly as the air velocity at the sparger head decreased.

The small pressure disturbances observed in experimental data during the early stage of sparger discharging were not predicted in the simulated pressure histories. The simulated pressure remained nearly constant until air venting begins from LRR and then increases rapidly as shown in the Figures 3, 4 and 5. This is caused by the numerical modeling used in the calculation. The complete separation of the water and air assumed in calculation, but the air bubble contains certain amount of water due to highly irregular motion of fluid around air bubble surface.

The maximum peak pressure occurs during the second oscillation after complete air venting as observed in the experimental data. The predicted period of oscillations are in the range of the experimental data. The calculated maximum positive peak pressures are approximately 3.5×10^{5} Pa, 2.2×10^{5} Pa and 1.4×10^{5} Pa, respectively. But the maximum peak pressures of the Unit Cell Test are in the range of $0.5\text{-}1.0\times10^{5}$ Pa. The over-prediction of the maximum peak pressure are caused by the discharge velocity of air at the choking condition, the critical velocity of air discharge consistent with the sparger design must be used to ensure the sparger performance.

Figures 6 shows the air bubble formation and its shape change during the air venting process at the various stages of Case A. The stages chosen are (a)the time of air venting from the LRR, (b)time of air venting from the sparger head, (c)time of maximum negative pressure, (d)time of medium pressure and (e)time of maximum positive pressure. During the air discharge period, the two air bubbles are formed at the two discharge locations, LRR and sparger head. The pressure fluctuations occurred in the first oscillation of the pressure history are caused by the time difference in air

discharge at the LRR and sparger head and by the interactions of these two bubbles. The figures also show the strong coherency of the air bubble until the time of maximum pressure which occurs the diffusion of air into the water mass. The volumetric oscillation of the air bubble between maximum negative and maximum positive pressure is also clearly shown in Figure 6.

Pressure distributions in the water pool are shown in Figure 7. The figures plotted pressure distributions at the time of the maximum negative pressure(a), maximum positive pressure(b) during the compression and expansion of air bubble. Figure 8 shows the pressure profile at wall at the maximum positive and negative pressure. This figure shows the linear style variation of pressure with the height in the tank.

Figure 9 shows the velocity vectors at the time of the maximum negative(a) and positive(b) pressure. At the time of the maximum positive pressure, the bubble at the sparger head is in the state at or near its maximum compression, while the LRR bubble starts to expand again. At the time of the maximum negative pressure, the sparger head bubble is in the state at or near its maximum expansion, while the LRR bubble starts to be compressed again. This explanation was derived from the observation of the velocity vectors downward from the LRR bubble toward the sparger head bubble. This explanation is also supported by the pressure distributions in Figures 7 and 8.

5. Conclusions

A numerical study was performed using preleased FLUENT V4.5 to investigate the applicability of CFD model to the IRWST hydrodynamic analysis during the sparger air venting for KNGR. Transient calculations were performed with the compressible VOF model on the selected ABB-Atom Unit Cell Test data. The analysis was focused on the reproduction of the bubble formation and its shape change and the time varying pressure history during the air venting from the sparger.

The simulation using FLUENT V4.5 reproduces some basic features of the flow such as bubble formation and pressure oscillation in the water pool reasonably well. The code, however, over-predicted the maximum peak pressure. The maximum peak pressure acceptable for the conservative evaluation of the sparger performance was obtained by reducing the air discharge velocity. This indicates that the air vent velocity is the most influential parameter on the maximum peak pressure.

From the result of the analysis, it may be concluded that FLUENT V4.5 can be used for the KNGR sparger performance analysis in general. However, the direct application of FLUENT code should be in careful manner. The applicability of FLUENT code to the analysis of the highly complicated phenomenon will be examined further by comparing the calculation results with test data and refining intrinsic modeling.

6. Acknowledgement

This study has been carried out under the KNGR development program by KEPCO

7. References

1. J. Fredell and Kemppainen, "Experimental investigation of relief valve vent clearing phenomena, KVB 75-643, ABB Atom, November 3, 1975
2. FLUENT user's guide version 4.3, Fluent Inc. January 1995
3. "ABB Atom Studsvik safety relief valve discharge tests(1974-1975)", videotape from high speed film, ABB-Atom, 1975
4. F. J. Moody, "Introduction to unsteady thermofluid mechanics", John Wiley & Sons Inc. 1990.

Table 1. Hydraulic Characteristics of the Sparger

items	Test Area(m^2)	Grid Area(m^2)	Inertial Resistance Factor (m^{-1})
LRR (PM 1)	0.00262	0.06283	water 5.0000E+02
			air & steam 5.0000E+04
Sparger Head (PM 2)	0.01131	0.31416	water 5.8000E+02
			air & steam 5.8000E+04
Bottom Hole (PM 3)	0.00049	0.00126	water 1.3000E+04
			air & steam 1.3000E+06

Table 2. Fixed velocity

items	Case A (m/sec)	Case B (m/sec)	Case C (m/sec)
LRR (PM 1)	water & air: 330 (13.8)	water & air: 100 (4.6)	water & air: 100 (4.6)
Sparger Head (PM 2)	water & air: 330 (11.8)	water & air: 100 (3.6)	water: 100 (3.6) air: 50 (1.8)

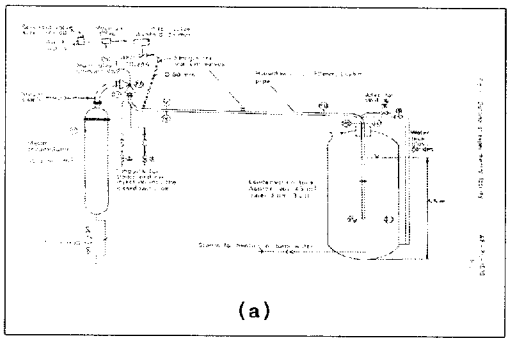

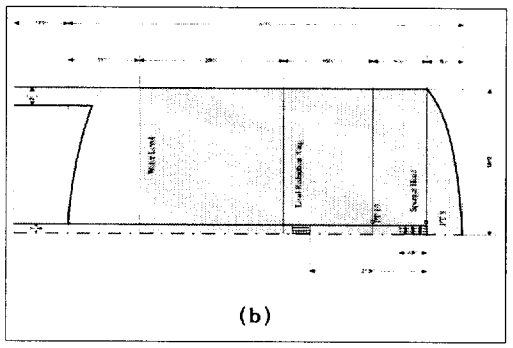

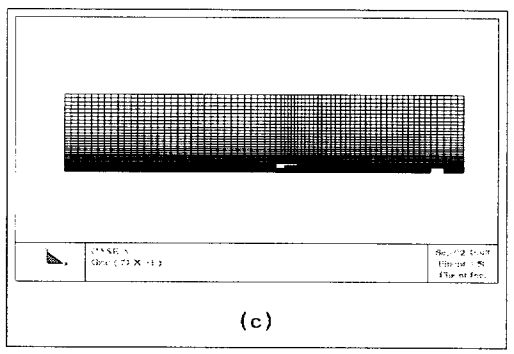

Fig. 1 Test facility and grid

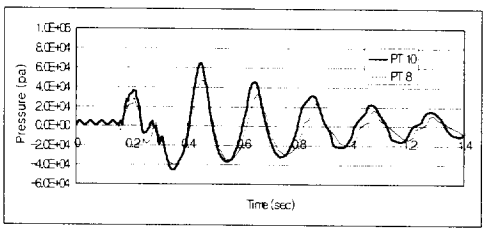

Fig. 2 Pressure history of Test

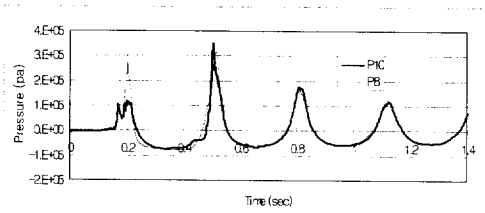

Fig. 3 Pressure history of Case A

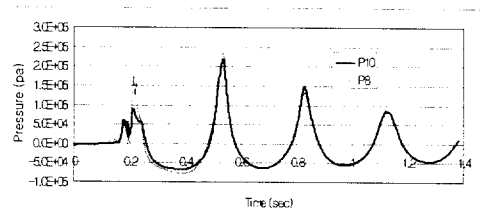

Fig. 4 Pressure history of Case B

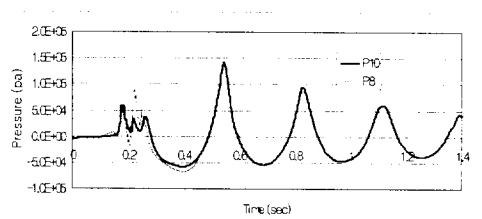

Fig. 5 Pressure history of Case C

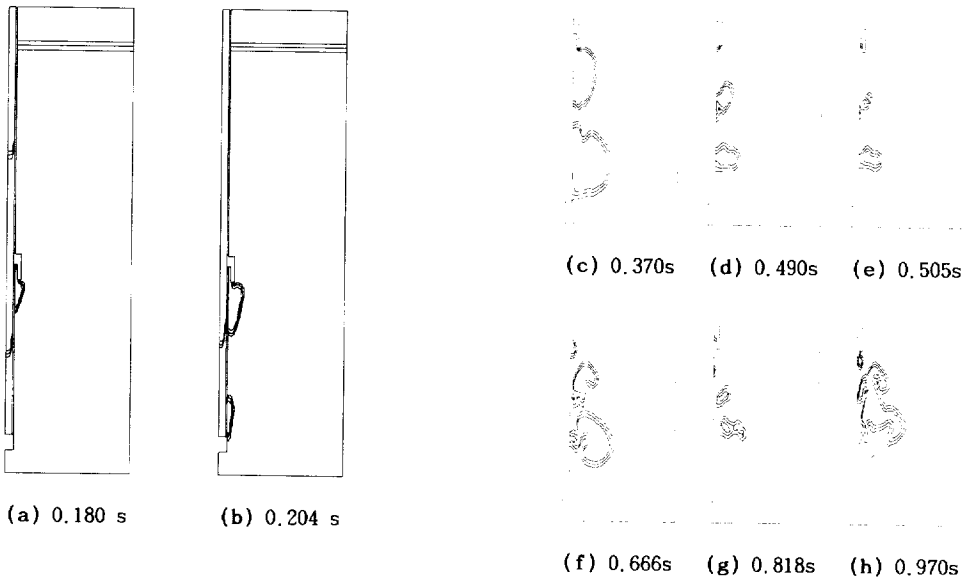

(a) 0.180 s (b) 0.204 s

(c) 0.370s (d) 0.490s (e) 0.505s

(f) 0.666s (g) 0.818s (h) 0.970s

Fig. 6 Contour of the air volume fraction (Case A)

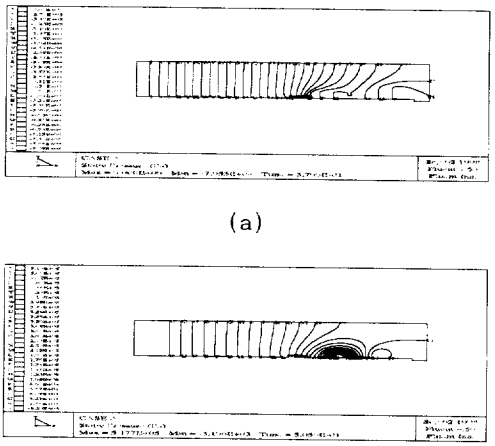

(a)

(b)

Fig. 7 Contour of the Pressure (Case A)

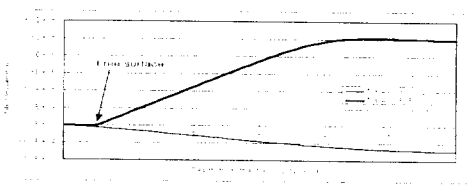

Fig. 8. Pressure Profile at Wall (Case A)

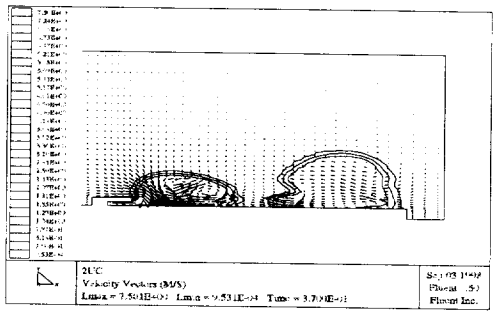

(a)

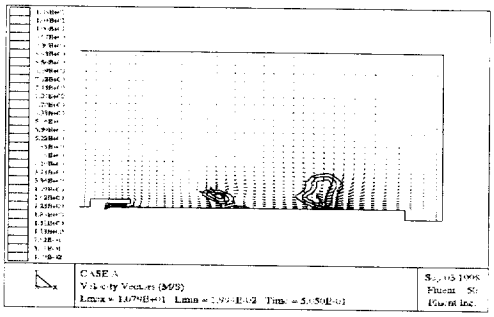

(b)

Fig. 9 Velocity vector (Case A)